Geophys. J. Int. (2005) **162,** 575–590 doi: 10.1111/j.1365-246X.2005.02580.x

Dynamic topography produced by lower crustal flow against rheological strength heterogeneities bordering the Tibetan Plateau

Marin K. Clark,[1,*] John W. M. Bush[2] and Leigh H. Royden[1]

[1]*Department of Earth, Atmospheric, and Planetary Sciences, Massachusetts Institute of Technology, Cambridge, MA* 02139, *USA. E-mail: mclark@gps.caltech.edu*

[2]*Department of Mathematics, Massachusetts Institute of Technology, Cambridge, MA* 02139, *USA*

Accepted 2004 December 23. Received 2004 November 30; in original form 2003 September 29

SUMMARY

Dynamic stresses developed in the deep crust as a consequence of flow of weak lower crust may explain anomalously high topography and extensional structures localized along orogenic plateau margins. With lubrication equations commonly used to describe viscous flow in a thin-gap geometry, we model dynamic stresses associated with the obstruction of lower crustal channel flow due to rheological heterogeneity. Dynamic stresses depend on the mean velocity ($\bar{U}$), viscosity (μ) and channel thickness (h), uniquely through the term $\mu\bar{U}/h^2$. These stresses are then applied to the base of an elastic upper crust and the deflection of the elastic layer is computed to yield the predicted dynamic topography. We compare model calculations with observed topography of the eastern Tibetan Plateau margin where we interpret channel flow of the deep crust to be inhibited by the rigid Sichuan Basin. Model results suggest that as much 1500 m of dynamic topography across a region of several tens to a hundred kilometres wide may be produced for lower crustal material with a viscosity of 2×10^{18} Pa s flowing in a 15 km thick channel around a rigid cylindrical block at an average rate of 80 mm yr^{-1}.

Key words: crustal rheology, dynamic topography, lower-crustal flow, Tibet.

1 BACKGROUND: LOWER CRUSTAL FLOW

The strength and mechanical behaviour of the lower continental crust is critical to the tectonic evolution and crustal dynamics of active orogens. A lower crust that is strong relative to the upper crust effectively transmits stress vertically through the crust, which requires that crustal motions will be directly coupled to mantle motions over very short length scales (tens of kilometres) (Royden 1996). However, in regions where the crust is hot or excessively thick, laboratory experiments predict that the middle or lower crust could contain a weak ductile zone, separating the more competent layers of the brittle upper crust from the rheologically stronger ductile upper mantle (e.g. Goetze & Evans 1979; Brace & Kohlstedt 1980; Kirby 1983). A depth-dependent rheology of the crust that includes such a weak layer drastically changes predicted patterns of surface deformation. A weak layer in the deep crust is not able to effectively transmit stresses vertically and causes the deformation of the crust to become decoupled from underlying mantle motions (e.g. Chen & Molnar 1983; Royden 1996; Roy & Royden 2000).

Many authors have proposed that where the lower crust is sufficiently weak, it will deform by channellized flow in response to lateral pressure gradients arising from differential crustal thicknesses or density contrasts within the crust (e.g. Bird 1991; Royden 1996; Bott 1999; Beaumont *et al.* 2001). Pressure-driven flow could allow for differential thickening of the upper and lower crust and possibly the long-distance transfer of crustal material over distances of >100 km (e.g. Synder & Barazangi 1986; Schmeling & Marquart 1990; Block & Royden 1990; Marquart 1991; Kruse *et al.* 1991; Royden *et al.* 1997; Clark & Royden 2000; McQuarrie & Chase 2000). Spatial separation of upper and lower crustal deformation precludes our ability to simply extrapolate surface deformation directly to the underlying deep crust and to infer changes in crustal thickness from surface structural data alone.

Key parameters governing the flow of weak lower crustal material are not yet well established, and are paramount to our understanding of crustal deformation. Insights gained directly from geophysical observations, and from exhumation of the deep crust, are limited because they offer only a 'snapshot' of the lower crust and therefore are a step removed from studying the dynamics of active processes controlling lower crustal behaviour. Outstanding questions include: Over what length scale does flow occur? What is the average flow velocity? What is the effective viscosity of the material in the channel? In order to constrain these parameters, we must be able to link temporal processes that we can measure (i.e. surface uplift, exhumation rates, crustal thickening, topography etc.) to lower crustal dynamics.

Modelling studies of active tectonic settings offers a means by which to investigate the dynamic behaviour of the lower crust during

*Now at: the Division of Geological and Planetary Sciences, California Institute of Technology, Pasadena, CA 91125, USA

orogenesis. In this paper we explore an actively deforming continental area in eastern Tibet where there is a juxtaposition of crustal regions with and without a weak ductile layer. We examine the manner in which non-lithostatic pressure gradients result in dynamically maintained (non-isostatic) excess topography as a consequence of the interaction of weak flowing crust with static regions of strong crust. By assuming that the flow is steady and constant, we use the modern topography to infer the properties of lower crustal flow.

2 MOTIVATION: CRUSTAL DYNAMICS AND TOPOGRAPHY IN TIBET

Strength contrasts in the continental crust may play an important role in the spatial distribution of crustal thickening and strain partitioning within the crust. Created by the ongoing continent–continent collision of India with Eurasia since ∼45 Ma, the Tibetan Plateau is an example of extreme regional topography over scales of hundreds to thousands of kilometres (e.g. Molnar & Tapponnier 1975; Le Fort 1975). The collision has resulted in the development of a low-relief but topographically high central plateau where the thickness of the crust has roughly doubled to about 70 km. The flatness of the central plateau has been attributed to the low strength of the lithosphere which prohibits the support of lateral pressure gradients that are produced by large topographic gradients (e.g. Bird 1991) and specifically may be attributed to the development of a low-viscosity layer in the middle or lower crust (e.g. Zhao & Morgan 1985; Bird 1991; Royden 1996). The hypothesis of a weak layer developed in the deep crust is supported by regional high heat flow beneath the plateau (Hu *et al.* 2000), a highly reflective and conductive middle crust observed in central Tibet (Nelson *et al.* 1996; Wei *et al.* 2001), and gravity data consistent with a model of a rheologically layered lithosphere beneath Tibet consisting of mechanically competent upper crustal and mantle layers separated by a weak low-viscosity zone in the lower crust (Jin *et al.* 1994).

Throughout the Alpine–Himalaya orogen, it has also been recognized that there are regions of the continental crust that virtually escape deformation and crustal thickening during active orogenesis. These blocks behave as rigid obstacles to ongoing deformation, often with concentrated deformation at their margins (e.g. England & Houseman 1985). In the region surrounding Tibet, these areas include the Tarim and Sichuan basins, as well as the Indian Shield. It has been proposed that these high-strength heterogeneities can be partly attributed to their 'tectonic age', inferred from their low lithospheric temperatures (e.g. Molnar & Tapponnier 1981; Hsu 1993) but may also be related to the lack of aqueous fluids, underplating of strong mafic material or thermal insulation by cold mantle lithosphere.

The elevated topography of the eastern plateau margin has been proposed to be the direct result of crustal thickening by weak, lower crustal material evacuated from beneath the central plateau (Royden *et al.* 1997; Clark & Royden 2000). The associated flux of this weak lower crustal material from beneath the central plateau into eastern Tibet suggests how crustal thickening along the eastern plateau and its margins has occurred despite a lack of significant shortening structures observed in the upper crust along the Longmen Shan/Sichuan Basin and southeastern plateau margins (Dirks *et al.* 1994; Burchfiel *et al.* 1995; Wang *et al.* 1998). Gradients in crustal thickness extending from the 60–70 km thick central plateau out into the 35 km thick eastern foreland (Li & Mooney 1998) are interpreted to be the driving force for crustal flow. Quantitative analyses of regional topographic slopes across the eastern plateau margin are determined by relating the topographic gradient of the margin to the strength of the channel material. Results indicate that the strength of the mid–lower crust beneath the southeastern and northeastern low-gradient margins of the plateau is very low (10^{18} Pa s if one assumes a 15 km channel) (Clark & Royden 2000). By contrast, the mid–lower crust beneath the steep eastern plateau margin which borders the Sichuan Basin is strong ($\geq 10^{21}$ Pa s for a 15 km channel). The regional topographic gradients as displayed on a smoothed elevation contour map and from 3-D digital topography perspectives show the continental crust 'flowing' from the high central plateau around the low-elevation Sichuan Basin, reflecting the flow of weak lower crustal material around a strength heterogeneity in the crust along the eastern margin of Tibet (Fig. 1).

3 MODEL: VISCOUS CHANNEL FLOW WITHIN THE LOWER CRUST AROUND CYLINDRICAL OBSTACLES

Effective lower crustal channel thicknesses have been estimated to be between 5 and 25 km (e.g. Wernicke 1990); however, when the system is modelled as simple Poiseuille (channel) flow, its dynamics are uniquely characterized by the inverse relationship between channel thickness and viscosity as h^2/μ where h is the channel thickness and μ is the Newtonian viscosity. For channel thicknesses between 10 and 15 km, estimates of channel viscosities range from 10^{17}–10^{20} Pa s and flow in the channel has been proposed to occur over length scales of tens to hundreds of kilometres (e.g. Block & Royden 1990; Kaufman & Royden 1994; McQuarrie & Chase 2000), and possibly over more than 1000 km (Clark & Royden 2000), with flow durations on the order of 10^6–10^7 yr. Flow within the channel is driven by horizontal pressure gradients, due to topographic gradients and variations in crustal thickness or density. In reality, flowing lower crustal material is likely not to have sharp, well-defined channel boundaries, but most geodynamic models approximate flow behaviour as Poiseuille flow (Bird 1991).

We model the lower crust as a viscous fluid bound within a channel with fixed rigid horizontal boundaries overlain by an elastic layer that is free to deform under the influence of the dynamic pressures generated within the channel. We assume that the total deflection of the upper surface is small relative to the total channel thickness, and that the channel thickness is small relative to the characteristic horizontal scale of the flow. Flow within the channel is presumed to be driven by horizontal pressure gradients associated with topographic gradients across the plateau.

In the absence of body forces, viscous flow of a Newtonian fluid is governed by the Stokes equations:

$$0 = -\nabla p + \mu \nabla^2 \mathbf{u}, \quad \nabla \cdot \mathbf{u} = 0 \tag{1}$$

where p is the dynamic pressure field, μ is the dynamic (Newtonian) viscosity and $\mathbf{u} = \langle u, v, w \rangle$ describes the flow in three dimensions.

The geometry of the channel allows us to make significant simplifications to the Stokes equation, which reduce to the lubrication equations commonly used to describe viscous flow in a thin gap. First, the dominant viscous stresses are associated with vertical velocity gradients. It follows that the vertical pressure gradient is much smaller than the horizontal pressure gradients, thus to a first-order approximation the pressure is a function of x and y alone. Therefore, the governing equations reduce to:

$$0 = -\frac{\partial p}{\partial x} + \mu \frac{\partial^2 u}{\partial z^2} \tag{2}$$

$$0 = -\frac{\partial p}{\partial v} + \mu \frac{\partial^2 v}{\partial z^2}. \tag{3}$$

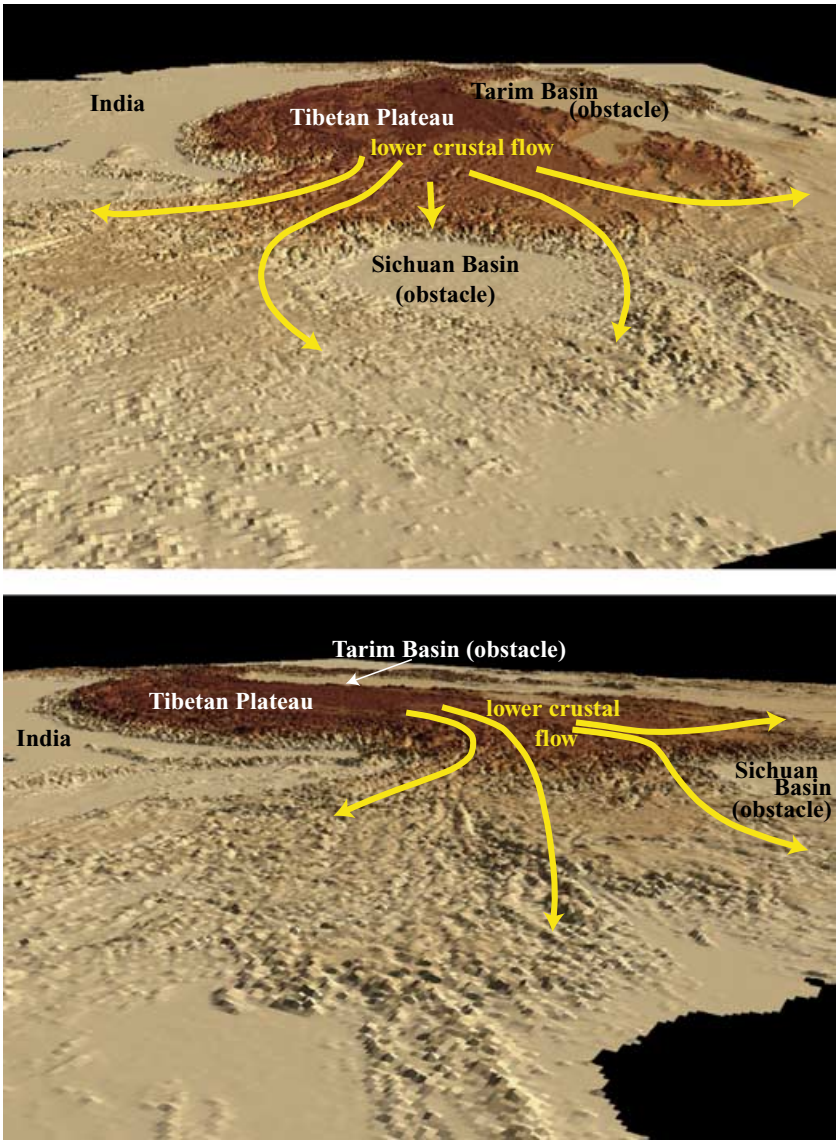

Figure 1. 3-D perspective of digital topography of eastern and southeastern Tibet, view to the west and northwest. The topographic gradient drives the flow of weak, lower crustal material around the rheologically strong Sichuan Basin, shown by yellow arrows.

These equations may be simply integrated with respect to z. Application of no-slip boundary conditions on the top and bottom of the channel ($z = \pm b$) and flow symmetry produces parabolic channel flow $\mathbf{u}$:

$$\mathbf{u} = -\frac{b^2}{2\mu}\nabla P\left[1 - \left(\frac{z}{b}\right)^2\right] \tag{4}$$

where $\mathbf{u} = \langle u, v\rangle$ and ∇P is the horizontal pressure gradient driving flow.

Our model for the weak, ductile channel layer corresponds to a Hele–Shaw cell bound above by a deformable elastic solid. The Hele–Shaw cell is commonly used to model flow in porous media and inviscid flows because of the peculiar feature that the flow at any given z is a pure, 2-D potential flow (an irrotational flow where flow is the gradient of a scalar potential). Because the pressure is a function of x and y only, it follows that $\partial v/\partial x = \partial u/\partial y$ and there are no streamwise velocity gradients. While the flow speed depends on z, the direction of flow is independent of z and the depth-averaged flow across the gap,

$$\overline{\mathbf{u}} = (\bar{u}, \bar{v}) = \frac{1}{2b}\int_{-b}^{b} \mathbf{u}\,dz,$$

satisfies Darcy's law:

$$\overline{\mathbf{u}} = -\kappa\nabla P \tag{5}$$

where $\kappa = b^2/3\mu$ is the effective permeability of the medium (Batchelor 1967; Acheson 1990; Furbish 1997).

We proceed by exploring the interaction between flow in our model lower crust and an 'impermeable' region (infinite μ) corresponding to an area of high crustal strength. We prescribe a unidirectional far-field flow $\overline{U}$ within the channel and examine the effect of an impermeable rigid obstacle corresponding to a rigid block or subregional crustal fragment modelled as a cylinder with its axis perpendicular to the direction of flow (Fig. 2a). One anticipates that the flow will be diverted around such obstacles. In 2-D, we consider unidirectional, steady flow past a circle with radius a and solve for the local pressure field created by the diverted flow. We apply a

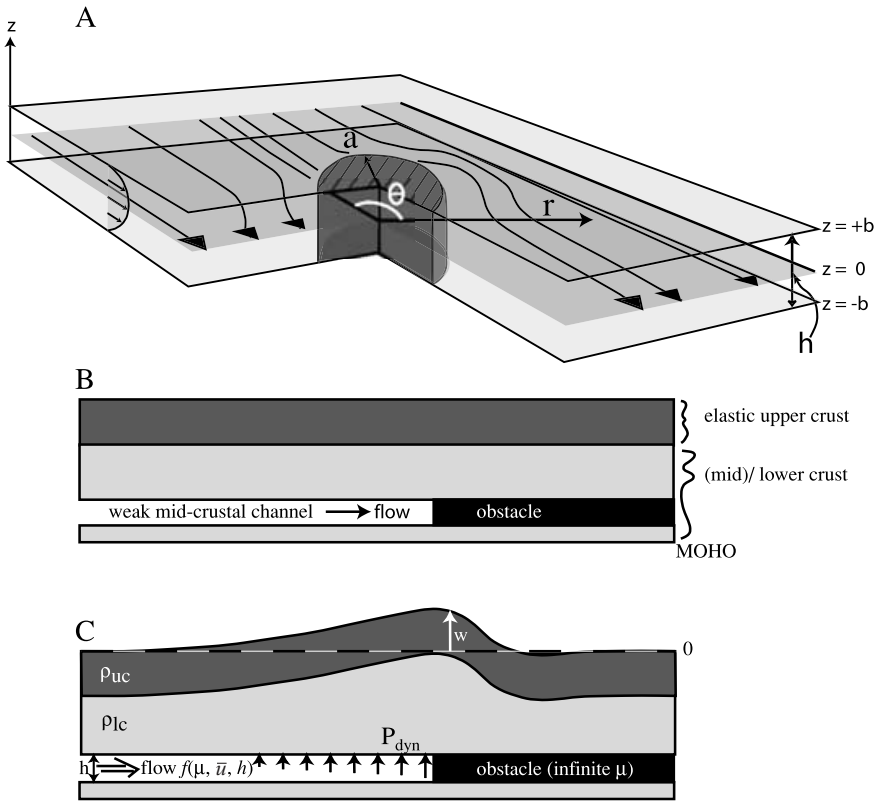

Figure 2. (a) Model geometry of Hele–Shaw cell flow (channel flow within a thin-gap geometry) past a rigid cylindrical obstacle with radius a. (b) Cross-sectional model geometry. (c) Dynamic pressure (Pdyn) calculated for the flow layer adjacent to the obstacle acts as a load on the elastic upper crust. Deflection of the upper crust (w) is observed as dynamic topography, which is damped by the elastic strength of the upper crust.

no-flux boundary condition at the surface of the circular obstacle ($\overline{u_r} = 0$ at $r = a$). Note that while no-slip conditions apply at $z \pm b$, this condition is not satisfied on the circle of the circular boundary. The appropriate solution for potential flow around a circle is given by:

$$\overline{u_r} = \overline{U}\left(1 - \frac{a^2}{r^2}\right)\cos\theta \tag{6}$$

and

$$\overline{u_\theta} = -\overline{U}\left(1 + \frac{a^2}{r^2}\right)\sin\theta \tag{7}$$

where $\overline{U}$ is the scalar value of the vertically averaged far-field flow, r is the radial distance and θ is the angle made with the direction of far-field flow (Fig. 2). The corresponding pressure field (excluding lithostatic pressure) is:

$$P = -\frac{1}{\kappa}\overline{U}\left(r + \frac{a^2}{r}\right)\cos\theta. \tag{8}$$

This pressure field is composed of two parts: a pressure relating to the background (far-field) flow and a local pressure field developed due to flow being diverted around the rigid obstacle. The latter can be thought of as a dynamic pressure or the dynamic load applied at the base of the overlying elastic crust where the dynamic pressure in dimensional form is equal to:

$$P_{\text{dyn}} = \frac{1}{\kappa}\overline{U}r\cos(\theta)\left(\frac{a^2}{r^2}\right). \tag{9}$$

In order to calculate the dynamic topography, we compute the flexural response of the upper crust in cross-section by applying a dynamic load to an elastic upper crustal layer and calculating the resulting deflection $w(x)$ (e.g. Turcotte & Schubert 1982) (Fig. 2b and c):

$$Dw_{xxxx}(x) + \rho g w(x) = P_{\text{dyn}}(x). \tag{10}$$

This model relies on several important assumptions. For simplicity, we assume that the channel walls are rigid and parallel. In reality, it is likely that the 'channel' (defined as the spatial domain over which the flow is active) is deflected or thickened near the boundary with the rigid block, and possibly elsewhere. Also, we only consider the effect of the dynamic pressure acting on the top of the channel. Theoretically, within the limitations of the Hele–Shaw model, there is an equal, and symmetrical, pressure acting on the base of the channel. Here, we assume the base of the channel to be rigid. The background pressure gradient driving regional, uniform velocity flow is not explicitly modelled as a regional topographic slope here, and instead a flow velocity is imposed on the channel material. The no-slip upper and lower boundary conditions are expected to be valid provided that pressure-driven channel flow is significantly faster than flow associated with differential motion of under- or overlying plates. Relative motion of these boundaries would impart an additional shear that would act to either enhance or retard flow and so influence the magnitude of dynamic topography (Beaumont *et al.* 2001). Finally, the calculated flexural response of the upper crust due to the dynamic load at depth assumes that the upper crust is a continuous plate. Using a broken plate would permit higher estimates of effective elastic thickness.

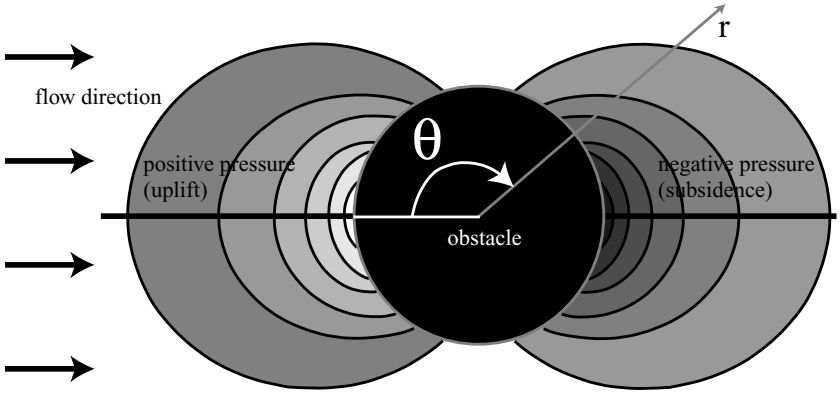

Figure 3. General model results showing map-view patterns of high and low dynamic pressures. Background flow is from left to right. Positive dynamic pressure (i.e. a load acting upwards on the top of the channel) is observed 'upstream' of the flow direction and predicts uplift at the surface. Negative dynamic pressure is observed 'downstream' and predicts subsidence at the surface.

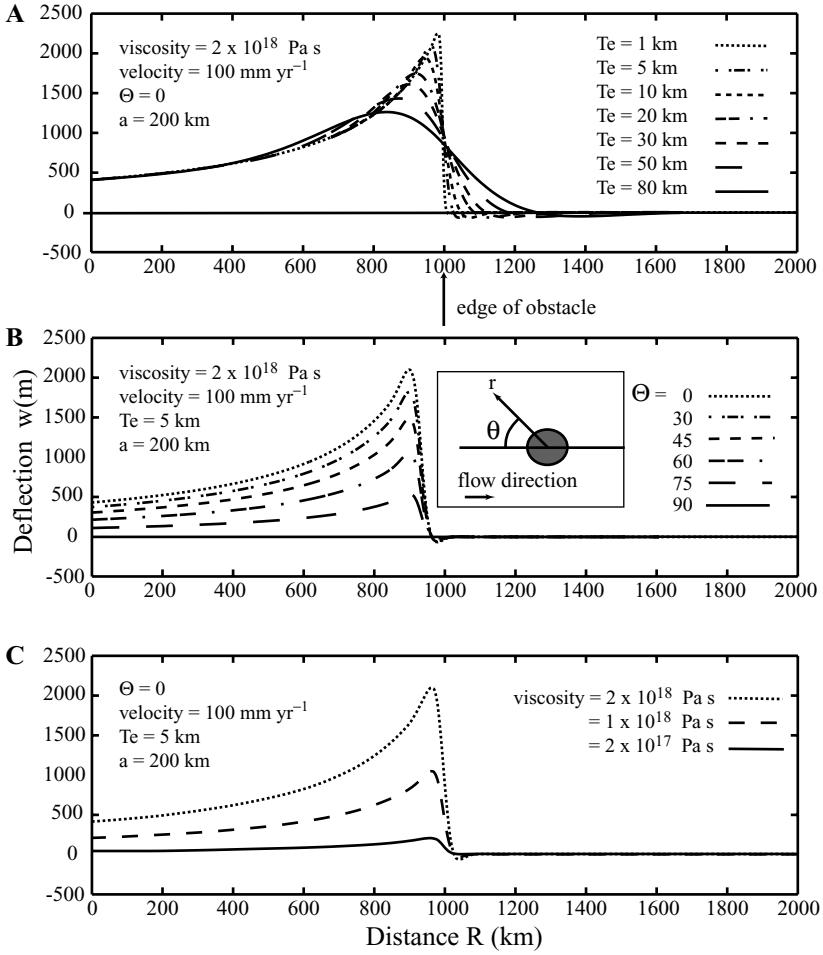

Figure 4. Example of dimensional cross-sectional deflection profiles (dynamic topography) produced by the model for the 'upstream' side of the obstacle. (a) Model deflection profiles for varying elastic strengths of the upper crust. Low flexural rigidities closely mirror the pressure distribution in the lower crustal layer. High flexural rigidities result in damped antiformal profiles. (b) Deflection profiles for varying profile azimuth with respect to flow direction. For example, $\theta = 0$ represents a profile oriented parallel to the flow direction, and $\theta = 90$ is oriented perpendicular to the flow direction. (c) Model profiles for varying viscosities. Acceptable deflection amplitudes are obtained with viscosities in the range of 2×10^{17} to 2×10^{18} Pa s.

4 MODEL PARAMETERS AND GENERAL RESULTS

Qualitatively, the dynamic pressure produced by the flow results in a first-order pattern of symmetric highs and lows oriented 'upstream' and 'downstream' of the obstacle respectively (Fig. 3). The regions of significant dynamic pressure are roughly crescent-shaped, with the highest-magnitude dynamic pressure located at the stagnation points of the flow adjacent to the boundary with the obstacle. The magnitude of the dynamic pressure decreases away from the obstacle

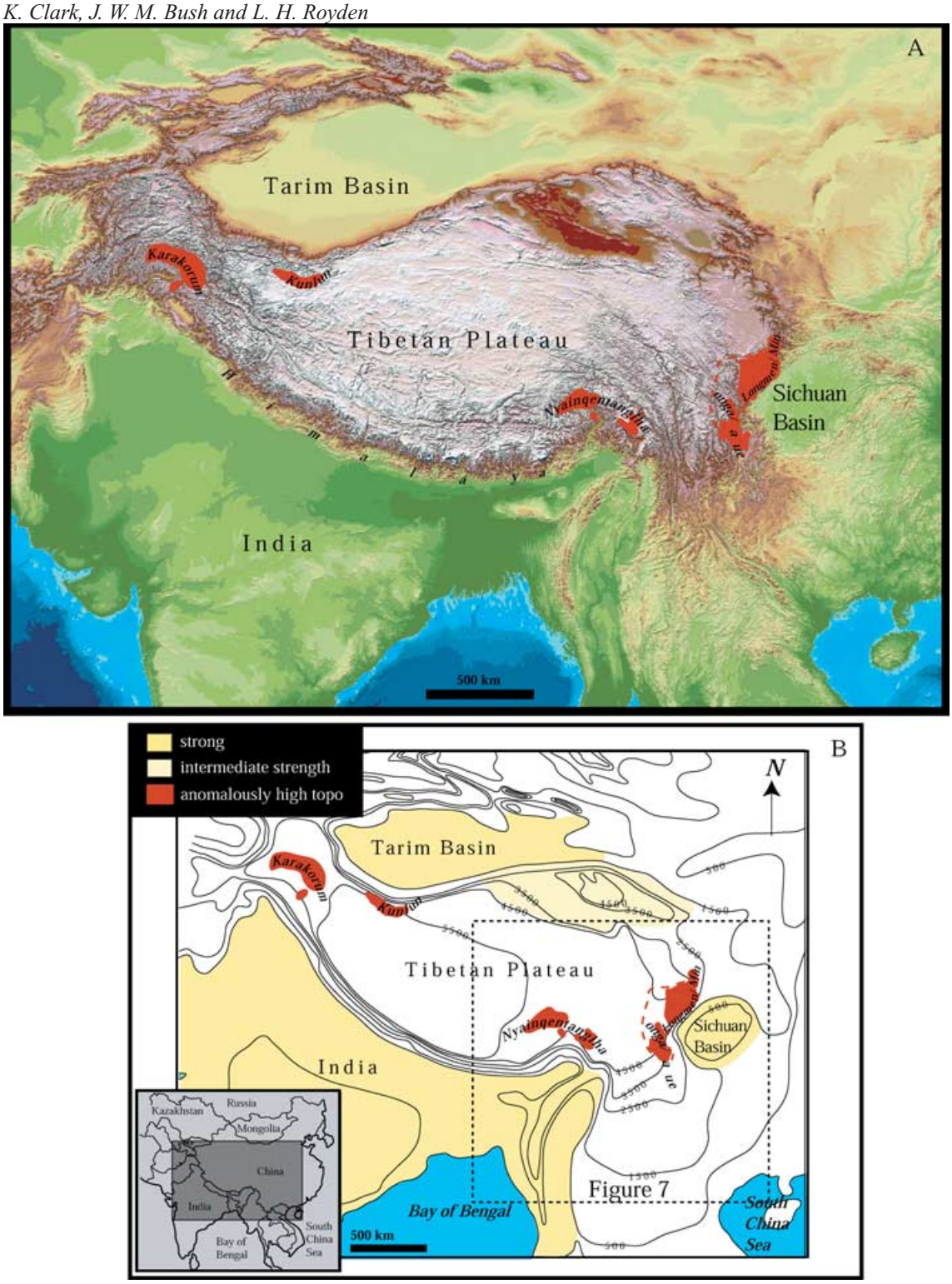

Figure 5. (a) Digital topography map of Tibet highlighting areas of anomalously high topography in excess of adjacent plateau elevations. (b) Smoothed contour elevation map derived from digital topography. Areas highlighted in dark yellow and light yellow indicate rheologically strong and intermediate strength crustal blocks respectively. White areas beneath the Tibetan Plateau and regions to the east have been suggested to contain a weak layer at mid to lower crustal depths. Regions in red indicate areas of anomalously high topography.

as the inverse of the radial distance from the centre of the obstacle, resulting in concave-up cross-sectional profiles (Fig. 4). The maximum dynamic pressure is highest along a section oriented parallel to the flow direction (stagnation point), and decreases as a cosine function to zero at an orientation perpendicular to the regional flow (eq. 4).

The dynamic pressure acts as a non-lithostatic load on the base of the upper crust and produces dynamic topography modified by the

Figure 6. Example of anomalously high topography in eastern Tibet. View east of the plateau surface at 4 km elevation (foreground) which is interrupted by the high peaks that define the Gonga massif at elevations of 5500–7556 m (background). Further east from the horizon, elevations decrease dramatically from the peak height of Gonga Shan (7756 m) into the Sichuan Basin (∼500 m). Photograph courtesy of ETH Library, Zürich archive of Professor Arnold Heim, 1930-1.

flexural strength of the upper crust. We express the flexural strength of the crust in terms of the effective elastic thickness (*Te*), which is related to the flexural rigidity D by $Te = [12D(1-\nu^2)/E]^{-3}$, where E and ν are Young's modulus and Poisson's ratio, respectively (e.g. Burov & Diament 1995). For low-flexural rigidities, the topography closely mirrors the dynamic pressure field. For increasing flexural strength, the cross-sectional shape of the predicted dynamic topography changes from a concave-up form that mirrors the calculated dynamic pressures to a damped, asymmetric antiform with increasing wavelength and decreasing amplitude (Fig. 4). The mechanical behaviour of the system is a function of the ratio h^2/μ; therefore we cannot independently determine both h and μ. For example, the same dynamic topography profile would result from a thin channel with a very low viscosity as from a much thicker channel with a higher viscosity.

5 COMPARISON OF MODEL RESULTS TO TOPOGRAPHY ALONG THE EASTERN TIBETAN PLATEAU MARGIN

5.1 General map view pattern compared with model results

Across the Tibetan Plateau we observe a spatial correlation between regions of anomalously high topography (in excess of surrounding plateau elevations) and areas of contrasting crustal strength (Fig. 5). In particular, these topographic anomalies occur adjacent to convexities (curvature of the plateau margin in plan view) to regions of strong foreland material that appears to 'indent' the weaker plateau. Areas of anomalous topography are roughly crescent-shaped in plan view and are deeply dissected by fluvial and glacial erosion, especially compared with the adjacent relatively uneroded plateau surface (Fig. 6). These areas are also associated with high rates of exhumation, and in some areas, detachment-style extensional faulting (Burg *et al.* 1998; Hubbard *et al.* 1995; Clark *et al.* 2001).

We find a good correlation between the position of the crustal 'obstacle', regional lower crustal flow direction (interpreted to be down the regional topographic gradient), and the geographical extent of anomalously high topography (Figs 1 and 5). For example, in the eastern syntaxial region, flow is interpreted to be moving southeastwards past the eastern syntaxis, and this geometry can be approximated as flow past the top half of a cylindrical obstacle (Fig. 7). Thus our model predicts dynamic highs on the 'upstream' side, in this case, west of the syntaxial corner. Near the Sichuan Basin, regional flow is interpreted to be flowing east directly against the southwest corner of the basin. This geometry is approximated as flow against the 'upstream' side of the cylindrical obstacle. In this case, positive dynamic topography is predicted to occur as a symmetric crescent located directly about the cylindrical axis (Fig. 7). We also observe a symmetry between the topographic patterns in eastern Tibet and those in the western plateau, where topographic highs at the western Himalayan syntaxis (Karakorum) and south of the Tarim Basin (West Kunlun Shan) are observed (Fig. 5).

5.2 Topographic analysis of the Sichuan Basin plateau margin

The topography surrounding the Sichuan Basin in eastern Tibet has been suggested to be the product of active lower crustal flow from central Tibet toward the east (Royden *et al.* 1997; Clark & Royden 2000; Kirby *et al.* 2000) and most closely resembles the model geometry of flow around a cylindrical obstacle (Fig. 1). River profiles and thermochronological data along the steep plateau margin (Longmen Shan) bordering the Sichuan Basin support localized, young and active uplift concentrated at the plateau margin front (Kirby *et al.* 2002, 2003), despite a lack of evidence for significant horizontal motion (>3 mm yr^{-1}) by surface shortening (Chen *et al.* 2000; King *et al.* 1997). Here we compare the pattern of focused vertical uplift in the Longmen Shan to the predicted patterns of dynamically maintained topography supported by pressure gradients

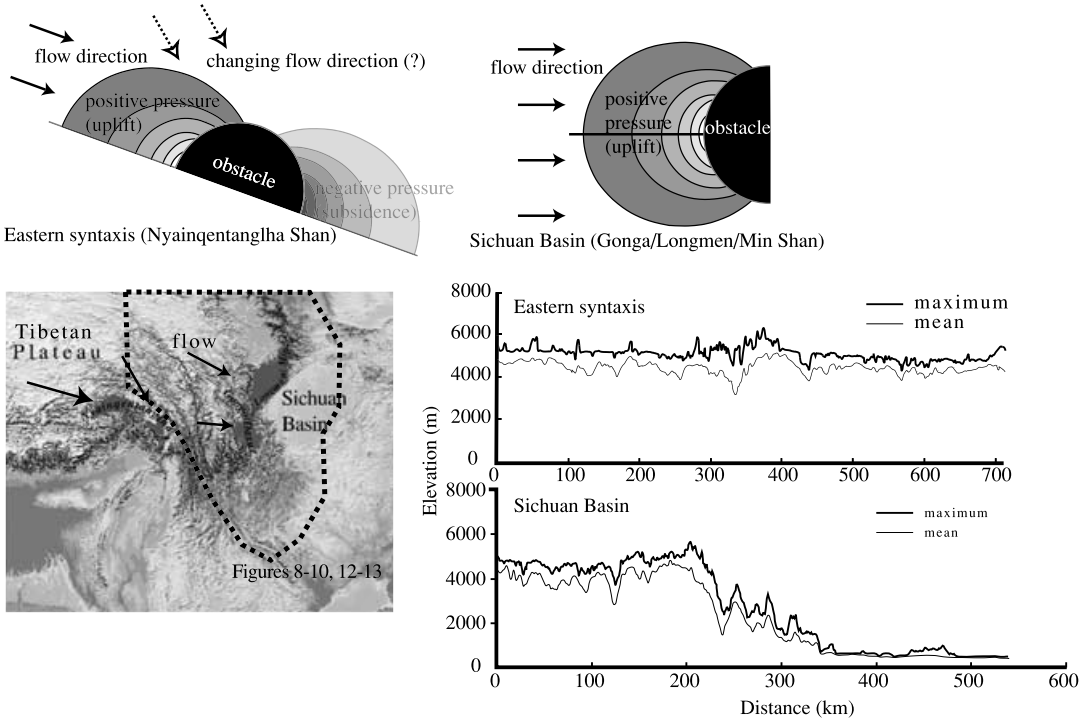

Figure 7. Model results compared with topographic observations in plan view and in cross-section. Near the eastern Himalayan syntaxis (Nyainqentanglha Shan), topographic gradients suggest that flow may be sideswiping the eastern promontory of the Indian craton. This geometry most closely corresponds to the top left quadrant of our model solution (flow is from left to right). Topographic gradients along the eastern margin suggest that flow may be occurring symmetrically against the southwest corner of the Sichuan Basin. This geometry most closely resembles the left half of our model solution (flow left to right). Sample topographic profiles from these two areas show locally elevated topography.

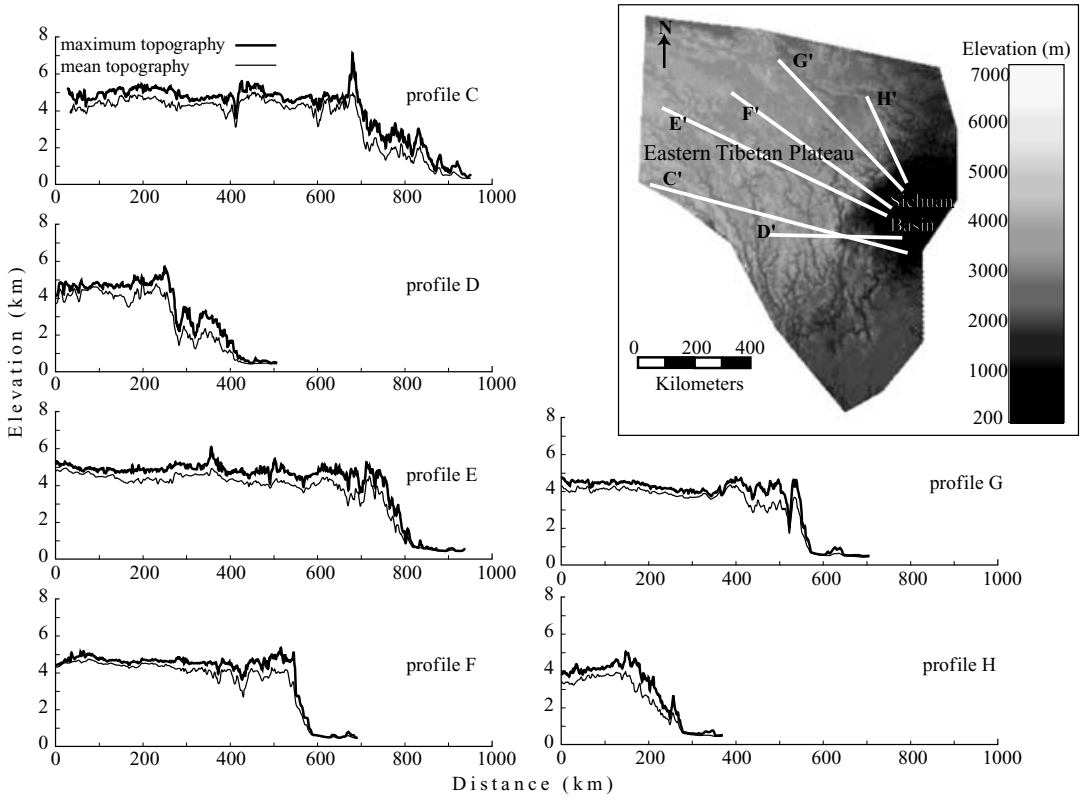

Figure 8. Maximum and mean swath profiles for the eastern plateau margin where the mean topography is averaged over a distance of 30 km perpendicular to the direction of the profile. This swath width is comparable to the focal mean grid used in Fig. 9. Max/mean swath profiles are taken in the same location as the focal mean profiles in Fig. 10.

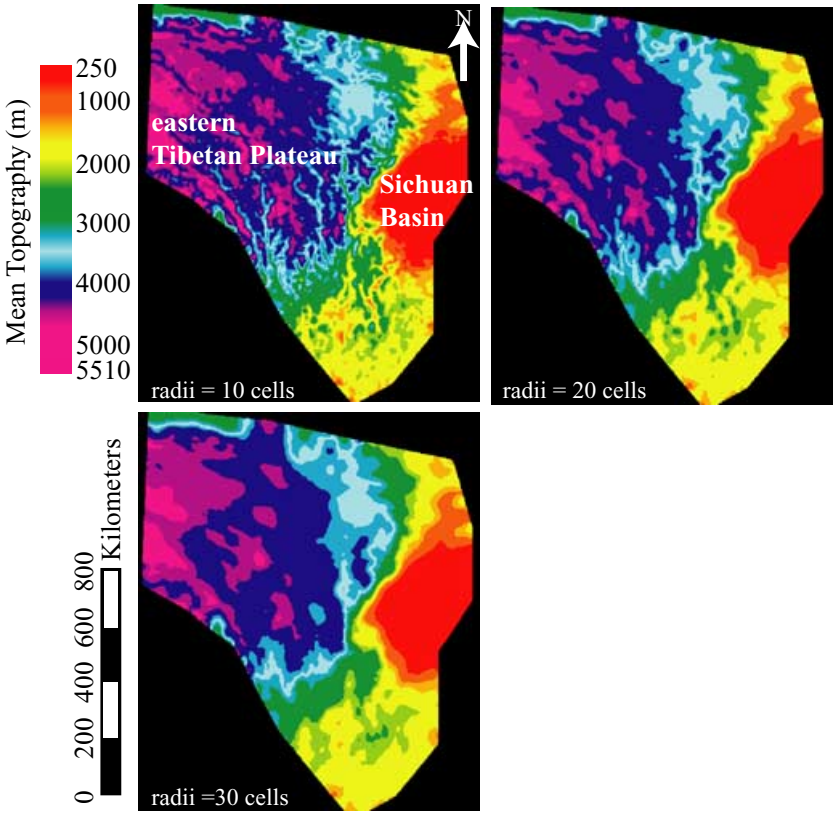

Figure 9. Three examples of mean topographic grids calculated from GTOPO30 digital topography (USGS 1993). Mean topography was calculated by averaging values over a circular neighbourhood domain. These plots show the effect of varying the radius of the averaging domain.

originating from crustal material flowing around the rigid Sichuan Basin.

The highest mountain peaks are concentrated at the margin front and profiles of maximum topography define smooth, concave-up profiles (Fig. 8) that can be considered as a minimum measure of surface uplift relative to the adjacent, modestly eroded plateau surface to the west. Localized peak uplift at the margin front suggests that lower crustal flow, coupled with erosion and extensional exhumation (observed in the Gonga Shan region and along strike of the Longmen Shan), may be responsible for creating and maintaining the Longmen Shan topographic escarpment. The predicted dynamic pressure arising from flow at depth should be reflected in the *mean* topography as well as the maximum topography (Fig. 8).

In order to extract dynamic topography from the mean topography we must calculate the far-field topographic gradient driving flow and subtract it from the observed topography in order to quantify any 'excess' topographic loads that reflect dynamic pressure within the lower crustal channel at depth. We present the following analysis which calculates the background mean topographic slope, from regions north and south of the Sichuan Basin, beneath which lower crustal material is predicted to be flowing over long spatial wave-length scales (Clark & Royden 2000). We assume that this slope is the far-field pressure gradient driving flow of lower crustal material in eastern Tibet. We compare this background mean profile with mean topographic profiles across the areas of anomalously high elevation and high local relief along the Longmen Shan/Gonga Shan region adjacent to the Sichuan Basin.

We use publicly available GTOPO30 digital topography (∼1 km resolution) (USGS 1993) to calculate a mean elevation grid using a 'focal mean' calculation, which determines the mean value for each cell (pixel) in the topographic grid. Fig. 9 shows examples of three such mean elevation maps for which the topography has been averaged over a circular neighbourhood domain with radii of 10, 20 and 30 grid cells (with the map projection used here, this equates to radii of ∼9, 17 and 26 km respectively). An averaging window of 10 cells retains much of the local variability and higher-wavelength topographic signature, which is likely to be supported by the flexural strength of the upper crust. An averaging window of 30 cells begins to average out salient features such as the steep plateau margin adjacent to the Sichuan Basin (length scale of 50–100 km). Thus, we propose that the mean elevation grid calculated from an averaging window with a radius of 20 cells represents the average crustal loads of interest. Profiles taken from the mean elevation grid across the southeastern and northeastern plateau margins are shown in Fig. 10.

Mean topographic profiles taken across the Sichuan Basin plateau margin are mapped onto the background mean topographic slope using segments of the profile that match the background slope (red) (Fig. 11). Profiles C and D cross the southern region of anomalously high topography (Gonga Shan). The elevations west and east of the high topography of the massif are used to align these profiles with the background mean profile (red) (Figs 11a and b). Profiles from farther north along the Longmen Shan and Min Shan front do not have low-slope plateau segments on either side of the anomalously high topography (profiles E, F and G). These profiles (E, F and G) were mapped to the background profile by aligning the steep front of the plateau margin (blue) with the steep segment on the Gonga profiles (profiles C and D) (Figs 11c–e). When we align profiles E, F and G in this manner, we find that the slope of the highest elevations on the profiles also matches the slope of the background

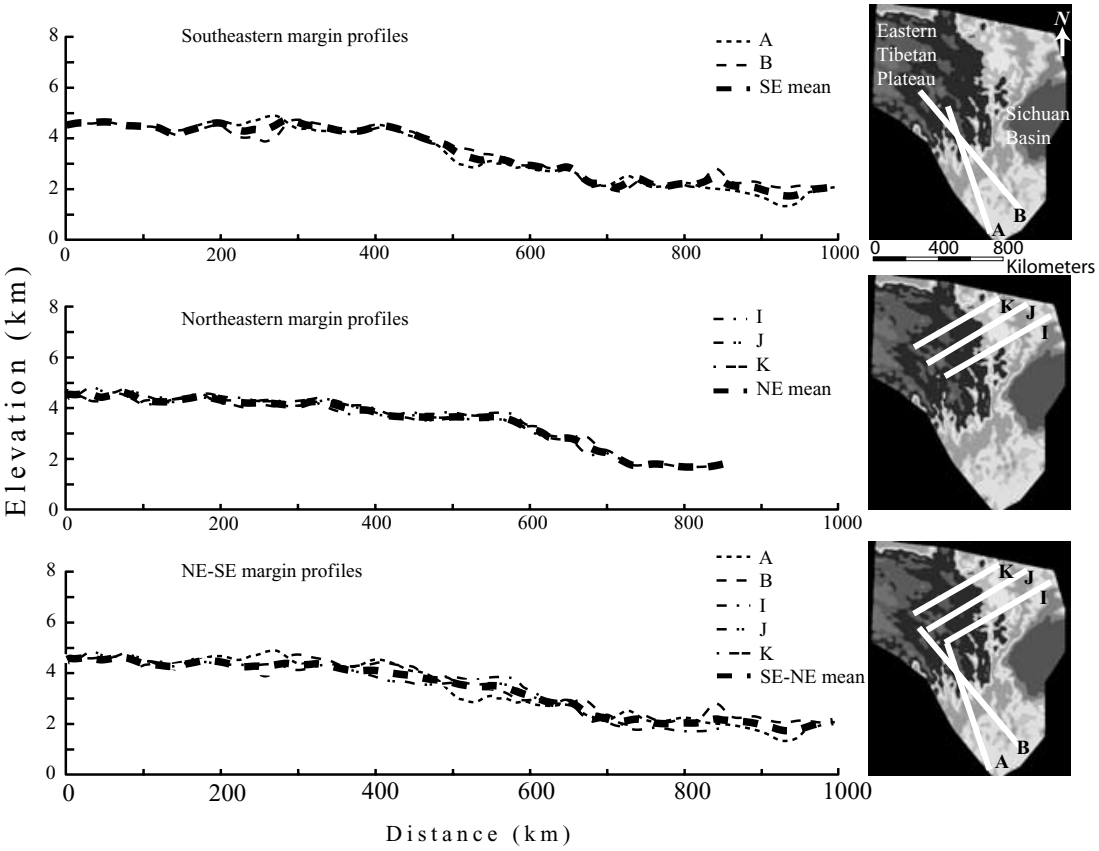

Figure 10. Averaged mean topographic profiles for the southeast, northeast and both margins combined.

profile. Profile H was aligned using both low-sloping segments that match the background profile (red) and a steep segment that matches profiles C–G (blue) (Fig. 11e). All profiles show additional steep segments at low elevations directly adjacent to the Sichuan Basin (green).

Once the individual profiles across the Sichuan Basin plateau margin are aligned with the background slope, they are subtracted from the background profile in order to calculate the amount of topography that is in excess of the far-field topographic slope driving flow (Fig. 12). We compare the result, referred to as a 'deflection profile' with model predictions for dynamic topography produced by flow past a rigid, cylindrical obstacle.

5.3 Comparison of topography with model results

The profiles shown in Fig. 13, from the Gonga Shan region (south) through the Longmen Shan and into the Min Shan (north), represent cross-sectional views of the topography oriented from $\theta = 0^\circ$ to 60° with respect to the flow direction, around a cylindrical obstacle of radius 200 km. Variations of velocity or viscosity within a factor of three to five produce results that mismatch the observed topography by several hundred metres. Profile C (oriented parallel to flow direction, $\theta = 0^\circ$), is fitted with model parameters of $\mu = 2 \times 10^{18}$ Pa s, $\bar{U} = 80$ mm yr^{-1} and $h = 15$ km (Fig. 13). It is important to bear in mind that we do not independently know the value of any of these parameters and that the dependence of the model profiles on viscosity, velocity and channel thickness enters exclusively through the group $[\mu\bar{U}/h^2]$. Using the parameters that best fit the amplitude for profile C, a best fit for the elastic strength (*Te*) of the upper crust is also determined (Fig. 13). The observed profiles show a best fit to low values for the effective elastic thickness of the upper crust ($Te = 1$–5 km), which match the sharp increase in topography at the basin margin. Higher values of *Te* produce a concave-down, rounded shape that no longer matches the amplitude/length scale ratio of the highest topography near the basin margin. Finally, using the parameters for $\bar{U}$, μ, h and *Te* determined from the model fits to profile C in Fig. 13, we compare variations in model azimuth with respect to the flow direction (θ) for several profiles along the Sichuan Basin plateau margin (Fig. 14). We match the best fit θ value for each profile. The best fit θ value for profiles C, D, E and G shows good agreement between model-predicted topography and observed topography for both the amplitude and length scale of the deflection profile, as well as the observed θ value assuming unidirectional flow against the Sichuan Basin. Profiles F and H match a much lower value of θ than is predicted, which suggests that these profiles have greater excess topography than is predicted by this model. Overall, the profiles show a gross progression in amplitude and length scale that matches the prediction of decreasing amplitude and wavelength from θ values of 0° toward 60° with respect to the flow direction. This prediction is in good accord with the highest observed topography located near the southwest corner of the Sichuan Basin in the Gonga Shan region and decreasing elevations toward the north along the Longmen Shan.

6 DISCUSSION

Modelling the subregional topography of the Sichuan Basin plateau margin in eastern Tibet offers an opportunity to estimate physical parameters that govern deep crustal deformation, assuming that flux of crustal material occurs over a fixed depth interval or channel. We

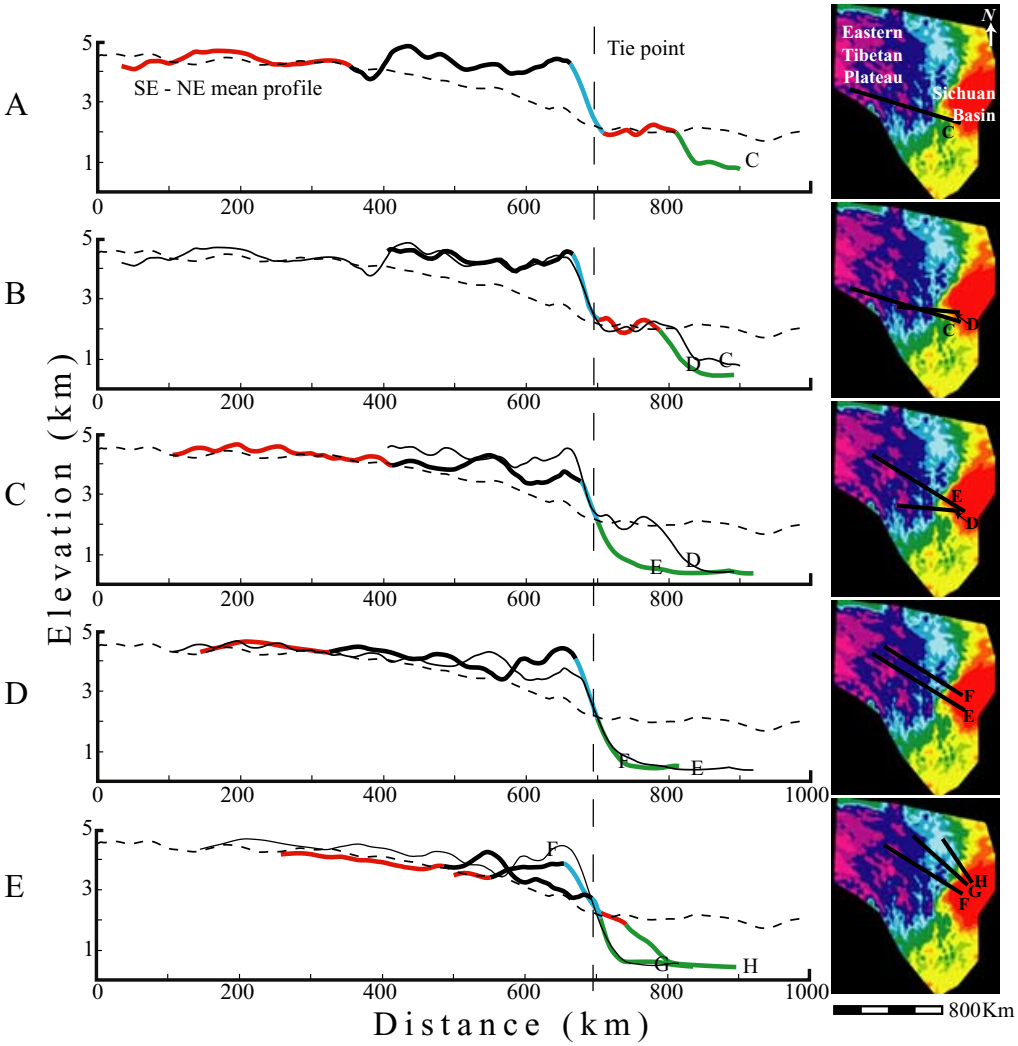

Figure 11. Comparison of individual mean topographic profiles with respect to the averaged southeast and northeast mean profile (background profile) for the gently sloping margins that surround the Sichuan Basin (dashed line). Segments highlighted in red represent portions of profiles that match on to the background mean profile. Profiles were aligned with the background slope by matching both low-slope segments (red) to the background and by matching up steep segments (blue). Profile segments in green represent the edge of the Sichuan Basin margin.

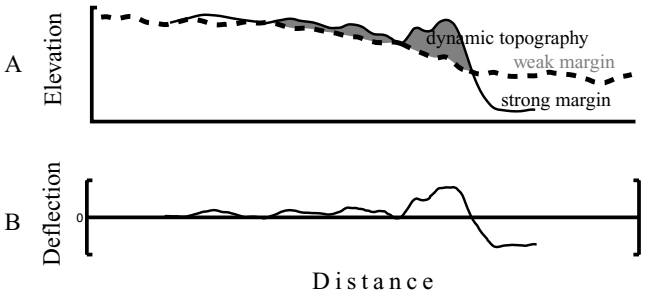

Figure 12. Example of dynamic topography calculation. (a) In the absence of a rigid crustal block (such as the Sichuan Basin), we may expect the topographic profiles across all of eastern Tibet to be relatively uniform and similar to the topographic profiles of the southeastern and northeastern plateau margins (weak margins). Higher topographic elevations are observed to have developed adjacent to the Sichuan Basin (strong margin). The difference between these two topographic profiles may represent dynamically maintained topography (grey) supported by the stresses originating from the diversion of crustal flow at depth around the undeforming, low elevation Sichuan Basin. (b) We obtain a 'deflection profile' by subtracting the topographic elevation across the strong margin from the profile taken across the weak margin.

can evaluate the consistency of these estimates with other calculations based on the regional topography of eastern Tibet which provides a means by which to evaluate observations at two different scales that may be linked to a common mechanism of ductile channel flow at depth. The averaged mean topographic gradient of the northeastern and southeastern plateau margins can be used to derive an independent estimate of the pressure gradient driving mid-crustal channel flow from central Tibet into the eastern foreland (Fig. 10). For these observed topographic gradients, we determine a velocity of $\bar{u} = \sim 20\,\mathrm{mm\,yr^{-1}}$ for a 15 km thick channel and a viscosity of $\mu = 2 \times 10^{18}$ Pa s. This estimate is compatible within a factor of four of the mean flow velocity of $\bar{U} = 80\,\mathrm{mm\,yr^{-1}}$ used to model the topography adjacent to the Sichuan Basin (for the same viscosity and channel thickness) in Section 5.

Assuming an initiation age for the uplift of eastern Tibet, estimates of viscosity and channel thickness were determined by forward modelling the regional topographic slopes of the eastern plateau margin from a 2-D flux model of pressure-driven channel material (Clark & Royden 2000). The cross-sectional topography of the southeastern and northeastern plateau margins can be modelled with a channel viscosity of $\sim 10^{18}$ Pa s (using 20 Ma as the initiation

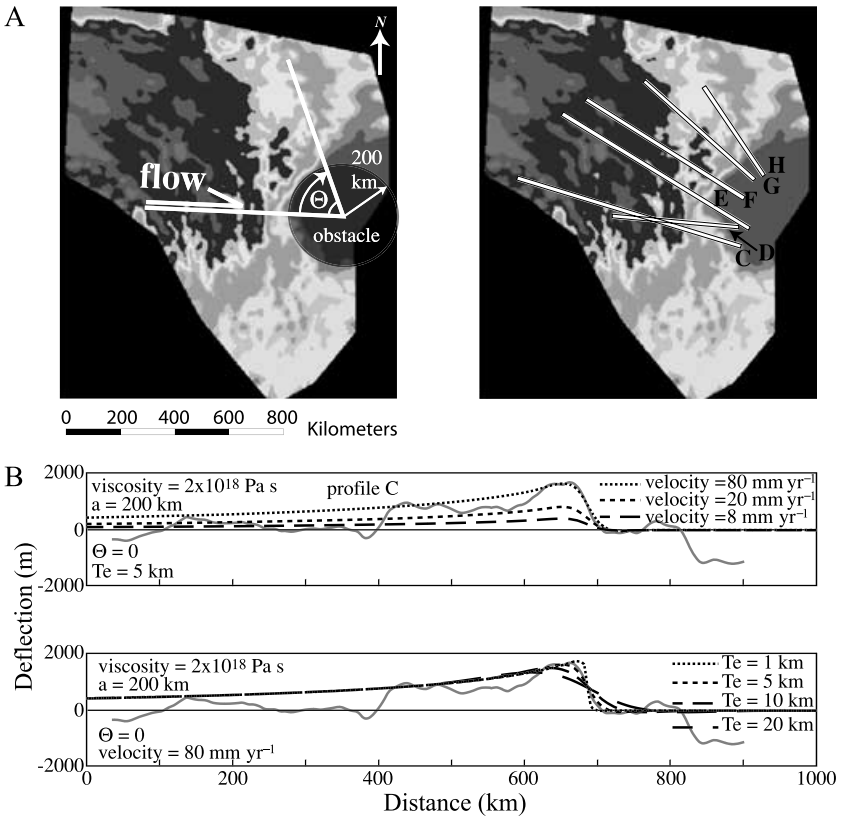

Figure 13. (a) Topography of the eastern Tibetan Plateau margin, showing the relationship of topographic mean profiles with respect to model geometry (left) and the location of individual profiles (right). (b) Comparison of model results to deflection profile C for varying velocity and varying effective elastic thickness (*Te*).

of uplift and a 15 km thick channel). We can also estimate viscosity and flow velocity from a mass balance calculation of eastern Tibet. Assuming that prior to uplift eastern Tibet was underlain by average-thickness crust (30 km) and that the present topography reflects crustal thickening in approximate Airy isostatic equilibrium, we can also determine an approximate total volume of added crustal material that may be the result of the addition of lower crustal material from beneath central Tibet into the eastern foreland (2.25×10^7 km^3) (Fig. 15). If we consider that the flux of material occurs through a crustal channel 15 km thick, this requires a viscosity of $\mu \sim 7 \times 10^{17}$ Pa s (for $t = 20$ Ma). These two estimates based on the topographic slope of the southeastern margin and the total crustal thickening of the plateau margin are in reasonable agreement (i.e. within an order of magnitude) with the model predictions of dynamic topography at the Sichuan Basin plateau margin presented in this paper. Moreover, our model estimates for channel thickness and viscosity are consistent with previously derived estimates for a weak, flowing mid–lower crustal layer described in the Basin and Range Province (i.e. 10^{17}–10^{20} Pa s for a 10–15 km thick channel) (e.g. Block & Royden 1990; Kruse *et al.* 1991; Kaufman & Royden 1994).

The Hele–Shaw model for lower crustal flow around a strength heterogeneity in the continental lithosphere differs from thin-sheet models that have previously examined the effect of rigid obstacles located within an otherwise weak, deforming lithosphere (England & Houseman 1985; Hsui *et al.* 1990). By definition, thin-sheet models predict uniformly distributed shortening of the viscous layer at a rigid boundary. The upwelling of weak lower crustal material flowing against a rigid obstacle may produce crustal thickening without surface shortening and induce extensional strain in the upper crust (Royden 1996; Shen *et al.* 2001). Therefore the presence of faults that accommodate margin-perpendicular extension may be a critical distinguishing feature that relates high-standing elevations to dynamically supported upwelling from a mid-crustal channel. The juxtaposition of high-standing topography, rapid surface uplift and exhumation, and in particular, the presence of extensional faulting and the exposure of young, anatectic mid-crustal rocks concentrated at rheological boundaries in Tibet (e.g. Hubbard *et al.* 1995; Roger *et al.* 1995; Burchfiel *et al.* 1995; Burg *et al.* 1998; Clark *et al.* 2001) may represent a common phenomenon related to rheological juxtaposition of strong crustal material against weak, flowing material.

Our model geometry is highly simplified: we assume unidirectional flow and rheological homogeneity at depth. The regional topographic gradients around the Sichuan Basin (and elsewhere in Tibet) indicate that the flow field is more arcuate than unidirectional because the topographic gradient slopes in all directions away from the highest topography in central Tibet. Also, we have assumed steady, uniform flow around the entire perimeter of the obstacle. In Tibet, we only observe high topography and interpreted flow interaction on the 'upstream' side of the rigid foreland regions, and do not observe flow completely encompassing obstacles as illustrated in the model geometry. A model of steady uniform flow may well approximate the upstream side; however, a time-dependent model describing the initiation of flow may illustrate differences that we have not yet explored. The structural complexity of the syntaxial regions precludes a simple relationship between fluid flow, topography and surface strain. Crustal thickening by upper crustal

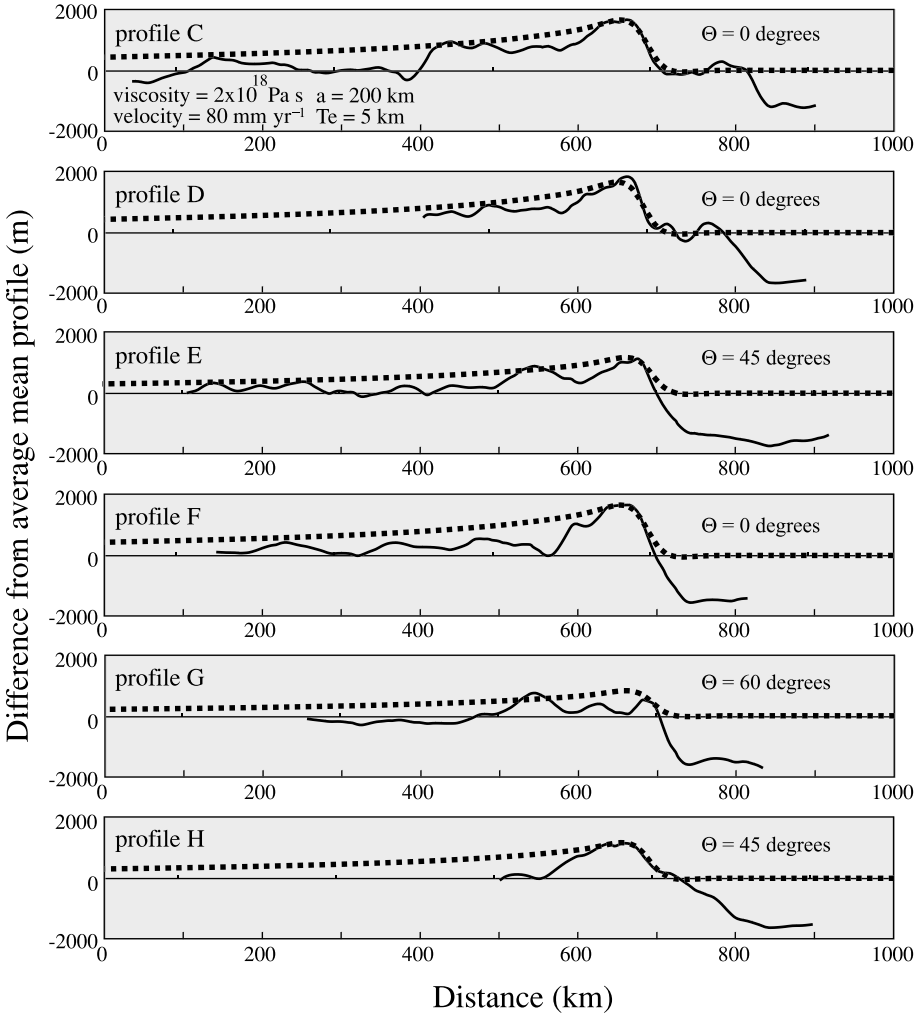

Figure 14. Comparison of model results with deflection profiles calculated for the eastern plateau margin for best fit θ value (orientation of profile with respect to lower crustal flow direction). Viscosity, flow velocity, obstacle radius and effective elastic thickness are constant for all profiles shown here. Profile locations are shown in Fig. 13(a).

structures that accommodate shortening perpendicular to the convergence direction undoubtedly plays a significant role in the modification of the topography, in particular along the southern (Himalayan) and northern plateau boundaries. More complicated geometries of rigid foreland regions, which may correspond to a specific geographical area, warrant further study.

7 CONCLUSION

Because active crustal flow occurs tens of kilometres deep in the crust, it cannot be directly observed. Understanding how lower crustal flow dynamics might be expressed in surface morphology and geology is one avenue for investigating the role of lower crustal behaviour during orogenesis. Our model allows us to make specific inferences concerning the exhumation and structural history of elevated regions where a significant portion of the observed topography is dynamically maintained by stresses due to the flow of weak material in the mid to lower crust. By exploiting the simple equations that govern Hele–Shaw flow, we are able to propose a simple leading-order expression for surface topography generated by these flows. Rigid cylindrical obstacles represent plan-view convexities commonly observed along the strike of orogenic belts. By presenting a geometry of flow past a cylindrical obstacle, we attempt to explore a general relationship between predicted dynamic topography and the presence of weak lower crustal flow in the vicinity of crustal strength heterogeneities, predicting first-order geometric patterns in map view and cross-sectional topography.

Our model geometry most closely resembles that of eastern Tibet adjacent to the Sichuan Basin where the contribution of upper crustal thickening to the development of high topography has been relatively minor and the shape of the Sichuan Basin is well approximated by a cylinder. Model results show that up to 1500 m of anomalously high topography at the Sichuan Basin margin may be accounted for by the flow of crustal material with a viscosity of 2×10^{18} Pa s at 80 mm yr^{-1} within a 15 km channel. These values are consistent with other estimates of viscosity and channel thickness values reported for Tibet and the Basin and Range Province (Block & Royden 1990; Kruse *et al.* 1991; Kaufman & Royden 1994; Clark & Royden 2000); this consistency supports the idea that lower crustal flow is a common phenomenon inherent to continental deformation.

The spatial distribution of areas of anomalously high topography in Tibet is consistent with our simple model of weak flowing material interacting with high-strength obstacles that inhibit flow and

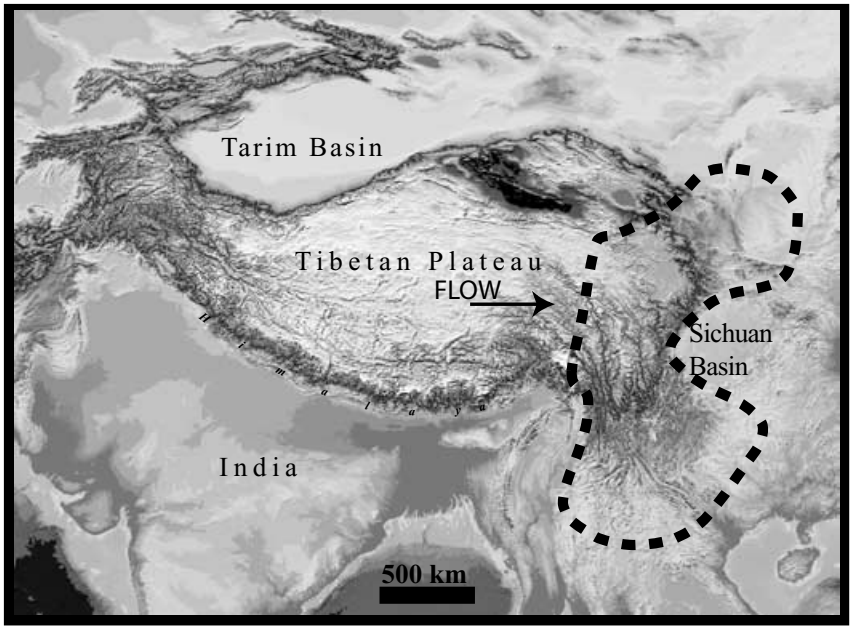

Figure 15. Dotted line represents the approximate area beneath which lower crust has been inferred to be added by flow from central Tibet.

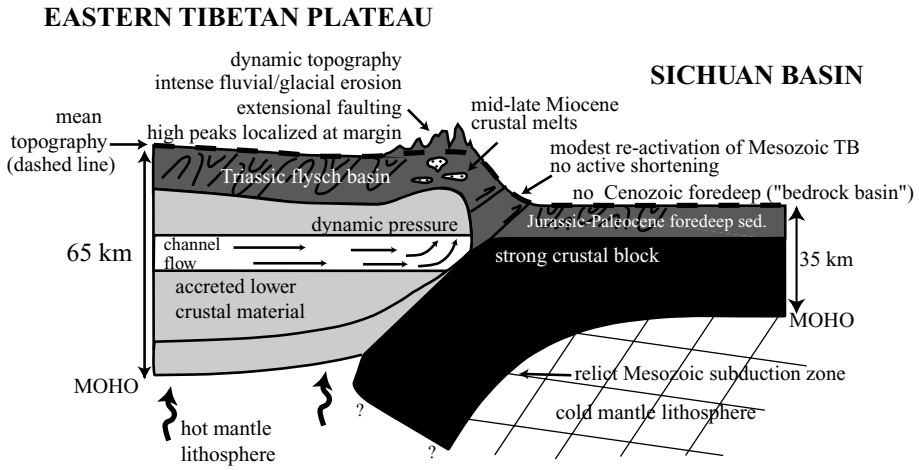

Figure 16. Schematic cross-sectional interpretation of the eastern plateau margin, at the latitude of the Gonga Shan massif. High topography has developed at the Sichuan Basin margin, despite modest shortening observed across reactivated Mesozoic structures, slow shortening rates (<3 mm yr^{-1}) shown by GPS data, and the lack of a Cenozoic flexural foredeep. High elevations adjacent to the basin margin may be supported by stresses in the middle/lower crust due to ductile flow of weak crustal material from elevated regions in central Tibet towards the low-elevation eastern foreland as flow is diverted around the Sichuan Basin. Limited deformation of the Sichuan Basin crust suggests it has behaved as a rigid block during Cenozoic tectonism related to the Indo-Eurasian collision. Observed extensional exhumation, rapid erosion, high peaks and mid-crustal anatexis localized at the Sichuan Basin margin in the vicinity of Gonga Shan may be related to dynamically maintained topography at the intersection of the flowing crustal material and the rigid crustal block. As evident from seismic tomography (Lebedev & Nolet 2003), the contrast in rheological properties between the eastern Tibetan Plateau and the Sichuan Basin may be related in part to the temperature (and/or presence of fluids) in the underlying mantle lithosphere.

cause the dynamically maintained 'excess' topography. These areas are also associated with extensional faulting and young magmatism which may also be related to the flow of weak mid–lower crustal material against high-strength heterogeneities in the surrounding foreland (Figure 16). Regional flow of lower crustal rocks against strength heterogeneities may explain the juxtaposition of high peaks and extensional faulting localized at orogenic plateau margins without needing to appeal to climatically-driven of high erosion rates (i.e. Beaumont *et al.* 2001).

Topographic evolution of an actively deforming region is an expected surface manifestation of lower crustal and shallow mantle dynamics. Availability of high-quality digital elevation models, development of quantitative laws to describe surface erosional processes and the ability to date and measure rates of surface change, underscore the importance of defining relationships that may exist between the evolution of topography and crustal/lithospheric deformation at regional scales, such as the development of dynamic topography derived from the process of lower crustal flow.

ACKNOWLEDGMENTS

The work in this paper was supported by a NSF graduate fellowship to MC, and NSF grants EAR-9814303, EAR-0003571 and EAR-9614970 to LR. JB gratefully acknowledges the financial support of the NSF through Career Grant CTS-0130465. We thank P. Molnar for his constructive review of this manuscript and B. C. Burchfiel, K. Whipple and M. House for their helpful comments and discussion on an earlier version. We also thank Z. Chen, X. Zhang and W. Tang of the Chengdu Institute of Geology and Mineral Resources and M. House for their assistance and expertise with geological research and field work in eastern Tibet.

REFERENCES

Acheson, D.J., 1990. *Elementary Fluid Dynamics,* Clarendon Press, New York, pp. 397.

Batchelor, G.K., 1967. *An Introduction to Fluid Dynamics,* Cambridge University Press, Cambridge, pp. 615

Beaumont, C., Jamieson, R.A., Nguyen, M.H. & Lee, B., 2001. Himalayan tectonics explained by extrusion of a low-viscosity crustal channel coupled to focused surface denudation, *Nature,* **414,** 738–742.

Bird, P., 1991. Lateral extrusion of lower crust from under high topography, in the isostatic limit, *J. geophys. Res.,* **96**(B6), 10 275–10 286.

Block, L. & Royden, L.H., 1990. Core complex geometries and regional scale flow in the lower crust, *Tectonics,* **9,** 557–567.

Bott, M., 1999. Modeling local crustal isostasy caused by ductile flow in the lower crust, *J. geophys. Res.,* **104**(B9), 20 349–20 359.

Brace, W.F. & Kohlstedt, D.L., 1980. Limits on lithospheric stress imposed by laboratory experiments, *J. geophys. Res.,* **85,** 6248–6252.

Burchfiel, B.C., Chen, Z., Liu, Y. & Royden, L.H., 1995. Tectonics of the Longmen Shan and adjacent regions, Central China, *Int. Geol. Rev.,* **37,** 661–735.

Burg, J.-P., Nievergelt, P., Oberli, F., Seward, D., Davy, P., Maurin, J.-C., Diao, Z. & Meier, M., 1998. The Nambshe-Barwa syntaxis: evidence for exhumation related to compressional crustal folding, *J. Asian Earth Sci.,* **16,** 239–252.

Burov, E. & Diament, M., 1995. The effective elastic thickness (Te) of continental lithosphere: what does it really mean?, *J. geophys. Res.,* **100**(B3), 3905–3927.

Chen, W.-P. & Molnar, P., 1983. Focal depths of intracontinental and intraplate earthquakes and their implications for the thermal and mechanical properties of the lithosphere, *J. geophys. Res.,* **88,** 4183–4214.

Chen, Z. *et al.*, 2000. Global Positioning System measurements from eastern Tibet and their implications for India/Eurasia intercontinental deformation, *J. geophys. Res.,* **105,** 16 215–16 227.

Clark, M.K. & Royden, L.H., 2000. Topographic ooze: building the eastern margin of Tibet by lower crustal flow, *Geology,* **28**(8), 703–706.

Clark, M.K., Royden, L.H., Bush, J., Burchfiel, B.C. & Zhang, X., 2001. Sub-regional dynamic topography and deformation of the lower crust by decoupled channel flow in Tibet, *EOS, Trans. Am. geophys. Un. Fall Meet.Suppl.,* **82,** abstract T11H-06.

Dirks, P.H.G.M., Wilson, C.J.L., Chen, S., Luo, Z.L. & Liu, S., 1994. Tectonic evolution of the NE margin of the Tibetan Plateau; evidence from the central Longmen Mountains, Sichuan Province, China, *J. Southeast Asian Earth Sci.,* **9**(1–2), 181–192.

England, P.C. & Houseman, G., 1985. Role of lithospheric strength heterogeneities in the tectonics of Tibet and neighbouring regions, *Nature,* **315,** 297–301.

Furbish, D.J., 1997. *Fluid Physics in Geology,*Oxford University Press, New York, pp. 476.

Goetze, C. & Evans, B., 1979. Stress and temperature in the bending lithosphere as constrained by experimental rock mechanics, *R. astr. Soc. Geophys. J.,* **59,** 463–478.

Heim, A., ETH-library, Zürich, Call no. Hs 494b:25 #290.

Hu, S., He, L. & Wang, J., 2000. Heat flow in the continental area of China: a new data set, *Earth planet. Sci. Lett.,* **179,** 407–419.

Hsu, K.J., 1993. Relict back-arc basins; principles of recognition and possible new examples from China, *Acta Petrol. Sinica,* **14**(1), 1–13.

Hsui, A.T., Wilkerson, M.S. & Marshak, S., 1990. Topographically driven crustal flow and its implication to the development of pinned oroclines, *Geophys. Res. Lett.,* **17**(12), 2421–2424.

Hubbard, M.S., Spencer, D.A. & West, D.P., 1995. Tectonic exhumation of the Nanga Parbat massif, northern Pakistan, *Earth planet. Sci. Lett.,* **133,** 213–225.

Jin, Y., Mc Nutt, M.K. & Zhu, Y., 1994. Evidence from gravity and topography for folding of Tibet, *Nature,* **371,** 669–674.

Kaufman, P.S. & Royden, L.H., 1994. Lower crustal flow in an extensional setting: constraints from the Halloran Hills region, eastern Mojave Desert, California, *J. geophys. Res.,* **99,** 15 723–15 739.

King, R.W. *et al.*, 1997. Geodetic measurement of crustal motion in Southwest China, *Geology,* **25**(2), 179–182.

Kirby, S.H., 1983. Rheology of the lithosphere, *Rev. Geophys. Space Phys.,* **21,** 1458–1487.

Kirby, E., Whipple, K.X., Burchfiel, B.C., Tang, W., Berger, G. & Sun, Z., 2000. Neotectonics of the Min Shan China; implications for mechanisms driving Quaternary deformation along the eastern margin of the Tibetan Plateau, *Geol. Soc. Am. Bull.,* **112**(3), 375–393.

Kirby, E., Reiners, P.W., Krol, M.A., Whipple, K.X., Hodges, K.V., Farley, K.A., Tang, W. & Chen, Z., 2002. Late Cenozoic evolution of the eastern margin of the Tibetan Plateau: inferences from 40Ar/39Ar and (U-Th)/He thermochronology, *Tectonics,* **21**(1), doi:10.1029/2000TC001246.

Kirby, E., Whipple, K.X., Tang, W. & Chen, Z., 2003. Distribution of active rock uplift along the eastern margin of the Tibetan Plateau: inferences from bedrock channel longitudinal profiles, *J. geophys. Res.,* **108**(B4), doi:10.1029/2001JB000861.

Kruse, S., Mc Nutt, M.K., Phipps-Morgan, J., Royden, L. & Wernicke, B.P., 1991. Lithospheric extension near Lake Mead, Nevada: a model for ductile flow in the lower crust, *J. geophys. Res.,* **96**(B3), 4435–4456.

Lebedev, S. & Nolet, G., 2003. The upper mantle beneath SE Asia from S-velocity tomography, *J. geophys. Res.,* **108**(B1), doi:10.1029/2000JB000073.

Le Fort, P., 1975. Himalayas: the collided range. Present knowledge of the continental arc, *Am. J. Sci.,* **275-A,** 1–44.

Li, S. & Mooney, W.D., 1998. Crustal structure of China from deep sounding profiles, *Tectonophysics,* **288,** 105–113.

Marquart, G., 1991. Finite element modeling of lower crustal flow: a model for crustal thinning variations, *J. geophys. Res.,* **96**(B12), 20 331–20 335.

McQuarrie, N. & Chase, C., 2000. Raising the Colorado Plateau, *Geology,* **28**(1), 91–94.

Molnar, P. & Tapponnier, P., 1975. Cenozoic tectonics of Asia: effects of a continental collision, *Science,* **189,** 419–426.

Molnar, P. & Tapponnier, P., 1981. A possible dependence of tectonic strength on the age of the crust in Asia, *Earth planet. Sci. Lett.,* **52,** 107–114.

Nelson, K.D. *et al.*, 1996. Partially molten middle crust beneath southern Tibet: synthesis of Project INDEPTH initial results, *Science,* **274,** 1684–1688.

Roger, F., Calassou, S., Lancelot, J., Malavieille, J., Mattauer, M., Xu, Z., Hao, Z. & Hou, L., 1995. Miocene emplacement and deformation of the Konga Shan granite (Xianshui He fault zone, west Sichuan, China): geodynamic implications, *Earth planet.Sci., Lett.,* **130,** 201–216.

Roy, M. & Royden, L.H., 2000. Crustal rheology and faulting at strike-slip plate boundaries; 2, Effects of lower crustal flow, *J. geophys. Res.,* **105**(3), 5599–5613.

Royden, L.H., 1996. Coupling and decoupling of crust and mantle in convergent orogens: implications for strain partitioning in the crust, *J. geophys. Res.,* **101**(B8), 17 679–17 705.

Royden, L.H., Burchfiel, B.C., King, R.W., Wang, E., Chen, Z., Shen, F. & Yuping, L., 1997. Surface deformation and lower crustal flow in eastern Tibet, *Science,* **276,** 788–790.

Schmeling, H. & Marquart, G., 1990. A mechanism for crustal thinning without lateral extension, *Geophys. Res. Lett.,* **17**(13), 2417–2420.

Shen, F., Royden, L.H. & Burchfiel, B.C., 2001. Large-scale crustal deformation of the Tibetan Plateau, *J. geophys. Res.,* **106**(4), 6793–6816.

Synder, D. & Barazangi, M., 1986. Deep crustal structure and flexure of the Arabian Plate beneath the Zagros collisional mountain belt as inferred from gravity observations, *Tectonics,* **5**(3), 361–373.

Turcotte, D.L. & Schubert, G., 1982. *Geodynamics: Applications of Continuum Physics to Geological Problems,* John Wiley, New York, pp. 450.

USGS (United States Geological Survey), 1993. *Digital Elevation Models, Data User Guide, 5,* pp. 1–50, US Geological Survey, Reston, VA.

Wang, E., Burchfiel, B.C., Royden, L.H., Chen, L., Chen, J., Li, W. & Chen, Z., 1998. *Late Cenozoic Xianshuihe-Xiaojiang, Red River, and Dali Fault Systems of Southwestern Sichuan and Central Yunnan, China,* Geological Society of America Special Paper 327, Geological Society of America, Boulder, CO, pp. 108.

Wei, W. *et al.*, 2001. Detection of widespread fluids in the Tibetan crust by magnetotelluric studies, *Science,* **292,** 716–718.

Wernicke, B.P., 1990. The fluid crustal layer and its implications for continental dynamics, in *Exposed Cross-sections of the Continental Crust,* pp. 509–544, eds Salisbury, M.H. & Fountain, D.M., Kluwer Academic, Dordrecht.

Zhao, W.-L. & Morgan, W.J., 1985. Uplift of the Tibetan Plateau, *Tectonics,* **4,** 359–369.